

ORIGINAL RESEARCH

Open Access



Localization of TSH-secreting pituitary adenoma using ^{11}C -methionine image subtraction

Daniel Gillett^{1,2*} , Russell Senanayake², James MacFarlane², Merel van der Meulen², Olympia Koulouri², Andrew S. Powlson², Rosy Crawford¹, Bethany Gillett³, Nick Bird¹, Sarah Heard¹, Angelos Koliass⁴, Richard Mannion⁴, Luigi Aloj^{1,5}, Iosif A. Mendichovszky^{1,5}, Heok Cheow¹, Wael A. Bashari² and Mark Gurnell^{2,6} 

Abstract

Background: Pituitary adenomas (PA) affect ~ 1:1200 of the population and can cause a wide range of symptoms due to hormone over-secretion, loss of normal pituitary gland function and/or compression of visual pathways, resulting in significantly impaired quality of life. Surgery is potentially curative if the location of the adenoma can be determined. However, standard structural (anatomical) imaging, in the form of MRI, is unable to locate all tumors, especially microadenomas (< 1 cm diameter). In such cases, functional imaging [^{11}C -methionine PET/CT (Met-PET)] can facilitate tumor detection, although may be inconclusive when the adenoma is less metabolically active. We, therefore, explored whether subtraction imaging, comparing findings between two Met-PET scans with medical therapy-induced suppression of tumor activity in the intervening period, could increase confidence in adenoma localization. In addition, we assessed whether normalization to a reference region improved consistency of pituitary gland signal in healthy volunteers who underwent two Met-PET scans without medical suppression.

Results: We found that the mean percentage differences in maximum pituitary uptake between two Met-PET scans in healthy volunteers were 2.4% for SUVr [cerebellum], 8.8% for SUVr [pons], 5.2% for SUVr [gray matter] and 23.1% for the SUVbw [no region]. Laterality, as measured by contrast–noise ratio (CNR), indicated the correct location of the adenoma in all three image types with mean CNR values of 6.2, 8.1 and 11.1 for SUVbw, SUVbwSub and SUVrSub [cerebellum], respectively. Subtraction imaging improved CNR in 60% and 100% of patients when using images generated from SUVbw [no region] and SUVr [cerebellum] scans compared to standard clinical SUVbw imaging.

Conclusions: Met-PET scans should be normalized to the cerebellum to minimize the effects of physiological variation in pituitary gland uptake of ^{11}C -methionine, especially when comparing serial imaging. Subtraction imaging following endocrine suppression of tumor function improved lateralization of PA when compared with single time point clinical Met-PET but, importantly, only if the images were normalized to the cerebellum prior to subtraction.

Keywords: ^{11}C -methionine PET, Human pituitary tumors, Normalization, Subtraction imaging

Background

Although the majority of pituitary tumors are benign (pituitary adenomas, PA), they can be associated with significant morbidity and increased mortality and affect approximately 1:1200 of the general population [1]. Symptoms and signs may be due to compression of adjacent anatomical structures (e.g., superior extension

*Correspondence: daniel.gillett@addenbrookes.nhs.uk

¹ Department of Nuclear Medicine, Cambridge University Hospitals NHS Foundation Trust, Cambridge Biomedical Campus, Hills Road, Cambridge CB2 0QQ, UK

Full list of author information is available at the end of the article

compressing the optic chiasm with resultant visual loss) and syndromes associated with hormone excess [e.g., growth hormone (GH) in acromegaly; ACTH in Cushing Disease; thyroid-stimulating hormone (TSH) in thyrotropinomas (TSHomas)] or insufficiency due to failure of the normal pituitary gland (hypopituitarism) [2]. It is not surprising then that many patients with pituitary tumors report significantly impaired quality of life, even worse than for some cancers [3, 4]. Medical treatment can be very effective in certain PA subtypes (e.g., dopamine agonist for prolactinomas), but surgery remains the preferred management option for many patients (e.g., acromegaly, Cushing Disease, thyrotropinoma), aiming to preserve/restore vision and/or permanently remove the source of hormone excess [5–7]. However, transsphenoidal pituitary surgery (TSS) is challenging due to the close proximity of critical structures (e.g., internal carotid artery within the cavernous sinus) to the normal gland, which may limit the scope for surgical resection. Conventionally, gadolinium-enhanced T1- and T2-weighted MRI is used for preoperative localization of the tumor and to inform surgical planning. However, anatomical information obtained on conventional imaging does not always locate the tumor, especially in the case of pituitary microadenomas (<10 mm diameter) or when image contrast is low. Recently, we and others have demonstrated the potential clinical utility of molecular imaging to address this challenge [8–10]. Specifically, ^{11}C -methionine PET (Met-PET) has been shown to aid localization of newly diagnosed and recurrent tumors across the spectrum of PA subtypes [9, 10].

However, there remain a subgroup of patients in whom even the combination of MR and Met-PET yield equivocal findings. In this setting, the patient and clinician are faced with a difficult choice: Should they proceed to surgery with the likelihood that a more extensive exploration of the whole gland will be required in an attempt to localize the tumor—this approach is reasonable but may not achieve surgical cure if the tumor cannot be identified and carries a risk of damage to adjacent critical structures (e.g., carotid artery and normal pituitary gland). Alternatively, drug treatment can be deployed as primary therapy, but may be associated with side effects and is often required lifelong with attendant significant costs [e.g., >\$100 K per annum for somatostatin receptor ligand (SRL) therapy] [11]. Such treatment is often very effective. For example, TSHomas demonstrate somatostatin receptor (SSTR, predominately SSTR2 and SSTR5) expression [12]. Importantly, in a single illustrative case, suppression of the activity of the TSHoma (as confirmed by correction of the hyperthyroidism clinically and biochemically) appeared to correlate with reduction/extinction of the signal seen on Met-PET imaging

[9]. We therefore hypothesized that using a subtraction technique similar to that routinely used in SPECT for parathyroid adenoma [13] and ictal SPECT imaging [14–17] could aid pituitary tumor localization using Met-PET. These techniques use normalization to prepare the images for subtraction by either scaling the images, so the mean intensity in the two datasets is matched, or by scaling the image intensity using a reference region to create an image of ratios (known as standardized uptake value ratios—SUVrs) [18]. Ictal subtraction imaging has also been performed using a combination of SPECT and PET [19], while a novel application of PET subtraction imaging has successfully identified sepsis in multiple sites using ^{18}F -FDG imaging before and after antimicrobial therapy in a patient suffering recurrent sepsis episodes [16]. These subtraction techniques increase the contrast-to-noise ratio by reducing the surrounding signal that is consistent between scans while highlighting those areas that demonstrate change.

The subtraction imaging techniques described above differ in their approach; subtraction imaging to detect sepsis uses standardized uptake value—body weight (SUVbw) images, whereas parathyroid and ictal subtraction imaging uses normalized images. Here, we have applied both techniques and assessed their effectiveness to aid pituitary tumor localization compared to standard Met-PET. To effectively normalize the images, an appropriate reference region must be selected. Therefore, we compared three commonly used reference regions from other nuclear medicine studies of the central nervous system (cerebellum, pons and gray matter [18, 20, 21]) to determine which would yield the most consistent tracer uptake and should be used to normalize the datasets.

Methods

Population groups

Two groups of participants were included: six healthy volunteers and ten patients with a thyrotropinoma (subsequently confirmed histologically following pituitary surgery). The healthy volunteers were control subjects in a study which included an assessment of the reproducibility of Met-PET findings on scans performed at a one-month interval (Clinical Trial ID: *Research Registry* 2070). Data from healthy volunteers allowed the most appropriate reference region for normalization of the pituitary uptake to be determined. The patient group was used to explore which subtraction technique provided the clearest localization of the pituitary tumor (matched with findings at surgery). The cohort of patients with TSH-secreting pituitary adenomas included 2 men and 8 women, with a mean age of 58 years (range 27–75). In each case, the patient had confirmed hyperthyroxinemia (raised free thyroid hormone levels) with non-suppressed

TSH and met clinical and laboratory criteria for a diagnosis of autonomous tumoral TSH secretion [22]. All patients had microadenomas as reported by consultant neuroradiologists with expertise in pituitary disease and were subsequently reviewed at the regional pituitary multi-disciplinary team meeting. In four patients, these were visualized on standard clinical MRI [Spin Echo T1-weighted (T1SE) pre- and post-gadolinium and Fast T2-weighted SE (T2) FSE] and ranged from 6 to 10 mm in maximum diameter. A further three microadenomas were visualized on gradient recalled echo MRI (GRE, i.e., volumetric sequences used for PET to MRI registration) and ranged from 3 to 4 mm in maximum diameter. In the other three patients, the location of the microadenoma (4–5 mm in maximum diameter) could only be appreciated on GRE MRI when subsequently identified on Met-PET. Met-PET identified a clear adenoma in five patients, with suspected adenomas in a further three patients, but no definite abnormality in the remaining two cases. Each patient was treated with depot first generation somatostatin receptor ligand (SRL) (Lanreotide Autogel[®], 90 mg 4-weekly for 3 doses) as per standard clinical practice in preparation for surgery (to alleviate symptoms and mitigate the perioperative risks associated with uncontrolled thyrotoxicosis) [22]. In eight patients, the suspected site of a TSH-secreting microadenoma as visualized on MRI and PET was confirmed on histology following transphenoidal surgery. Two patients elected to continue with primary somatostatin receptor ligand therapy and both achieved sustained normalization of free thyroid hormone and TSH levels consistent with a tumoral origin of autonomous TSH secretion [23, 24]. These subjects were scanned according to clinical protocols prior to and following SRL therapy, which was anticipated to suppress Met-PET uptake in the tumor. This suppression of tumor function was confirmed clinically (resolution of symptoms) and biochemically (with normalization of thyroid hormone levels). Measurement of other pituitary hormones confirmed no other significant change in pituitary gland status.

Imaging procedure

Imaging was performed using a Discovery 690 PET/CT scanner (GE Healthcare, Chicago, Illinois, USA) 20 min (range 19–21 min) after administration of 382 MBq (range 293–411 MBq) of ¹¹C-Methionine. One 15 cm bed position centered on the subject's pituitary gland was acquired for 20 min. The images were reconstructed with OSEM iterative reconstruction using 3 iterations and 24 subsets, 128 × 128 matrix size, 2 mm Gaussian filter, scatter correction, CT-measured attenuation correction, time of flight and point spread function correction (SharpIR, GE). An unenhanced CT scan was acquired with 140 kV,

fixed mA of 220, a rotation speed of 0.5 s, a pitch of 0.984:1, 30 cm field of view, a slice thickness of 1.25 mm and a 1.25 mm spacing interval and reconstructed using filtered back projection.

MR imaging

MRI was performed with either a GE Optima[™] MR450w 1.5 Tesla scanner (GE Healthcare, Chicago, Illinois, USA) or a GE Signa[™] 3.0 Tesla scanner (GE Healthcare, Chicago, Illinois, USA) with a head coil using a fast spoiled gradient (recalled) echo (FSPGR) sequence. The sequence parameters were repetition time (TR) 11.5 ms, echo time (TE) 4.2 ms, slice thickness 1 mm and 256 × 256 matrix with 1 mm × 1 mm pixels. The images were acquired after a contrast injection of 0.1 mmol/kg gadobutrol (Gad).

Image registration

All registrations were performed in 3D Slicer [25] (version 4.10.2, 05–2019) using multi-modality rigid registration with six degrees of freedom, a maximum number of iterations of 1000 and a sampling ratio of 0.1%. To generate the required co-registered baseline and on-suppression Met-PET/MR images, the following steps were used (illustrated in Fig. 1).

1. The on-suppression MR (MR2) was registered to the baseline MR (MR1) resulting in MR2 [Co-Reg].
2. The baseline Met-PET (PET1) was registered to the baseline MR (MR1) to create PET1 [Co-Reg].
3. The on-suppression PET (PET2) was registered to the on-suppression MR (MR2 [Co-Reg]) resulting in PET2 [Co-Reg].
4. The PET2 [Co-Reg] was resampled into a matrix of the same size and shape as PET1 [Co-Reg] to create PET2 [Resampled].

Step 4 was required to enable voxel-wise manipulations to produce the subtraction images without the requirement for position and interpolation calculations while using the world coordinate system.

PET normalization

Normalized PET images (SUV_r) were created by dividing the voxel values of the PET image by the mean voxel value in a reference region (Fig. 2). This process was implemented in a scripted 3D Slicer module (Fig. 2). The regions were drawn using a local thresholding tool on one or two representative slices of the PET images. The location of this reference region was optimized by finding which of the potential reference regions used for normalization (cerebellum, pons and gray matter) gave the most consistent pituitary tracer uptake in scans from healthy volunteers imaged one month apart. Once the images

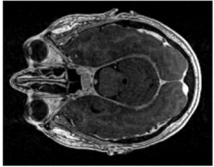
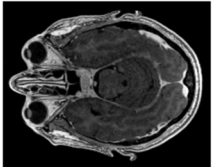
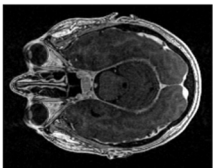
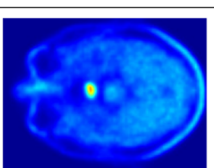
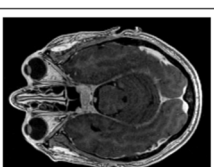
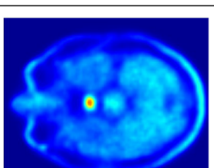
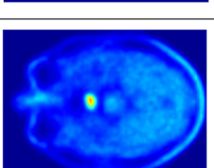
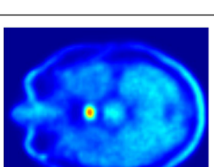
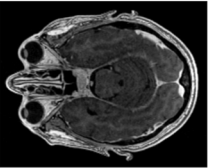
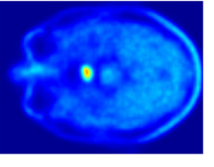
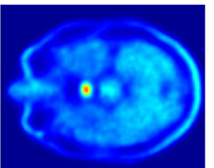
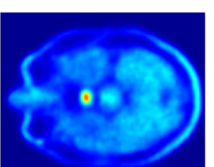
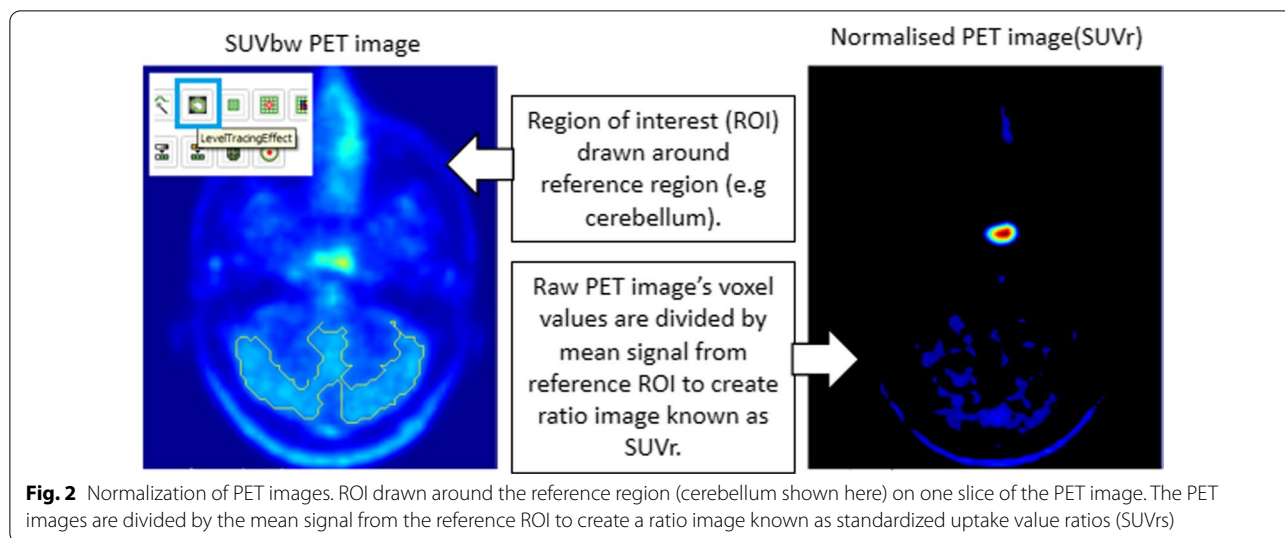
	Step 1		Step 2		Step 3		Step 4	
Inputs	 MR1 Fixed Volume	 MR2 Moving Volume	 MR1 Fixed Volume	 PET1 Moving Volume	 MR2 [Co-Reg] Fixed Volume	 PET2 Moving Volume	 PET1 [Co-Reg] Fixed Volume	 PET2 [Co-Reg] Moving Volume
Operations	Rigid Registration		Rigid Registration		Rigid Registration		Rigid Registration; resampling	
Outputs	 MR2 [Co-Reg] Registered Volume		 PET1 [Co-Reg] Registered Volume		 PET2 [Co-Reg] Registered Volume		 PET2 [Resampled] Registered Volume	

Fig. 1 Registration steps. Step 1: MR2 is registered to MR1 using rigid registration. Step 2: PET1 is registered to MR1 using rigid registration. Step 3: PET2 is registered to MR2 [Co-Reg]. Step 4: PET2 [Co-Reg] is registered to PET1 [Co-Reg] and resampled into a matrix of the same size and shape



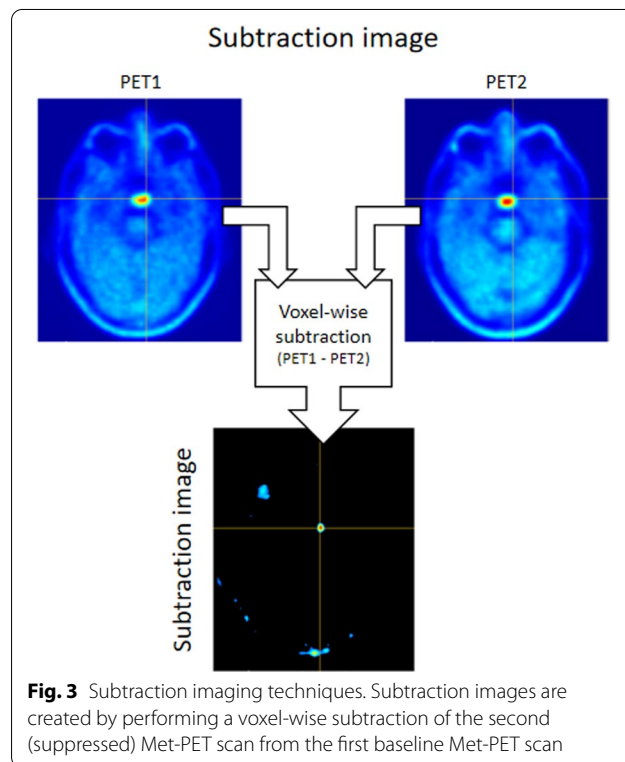
had been normalized to the reference regions, consistency was measured by finding the absolute percentage difference between the maximum signal in the pituitary gland at both time points. The region with the lowest mean absolute difference was considered the most appropriate region for normalization.

Subtraction images

Subtraction images were created by subtracting the on-suppression Met-PET image (PET2[Resampled]) from the baseline Met-PET image (PET1[Co-Reg]) (Fig. 3). This process was performed using SUVbw Met-PET images and the normalized SUVr (using the optimal reference region) Met-PET images to create two subtraction images for comparison (known as SUVbwSub and SUVr-Sub, respectively). This process was scripted using 3D Slicer’s native Python environment. The entire process, including registration, was completed in less than 5 min.

Assessment methodology

To quantitatively compare subtraction images using SUVbw images and SUVr images, ten patients who had confirmed lateralization of a microadenoma (<10 mm) were assessed using a semi-automated technique. This was undertaken by assessing lateralization using a modified contrast-to-noise ratio equation which selected the maximum signal from each side of the pituitary gland. The mid-line of the gland was defined on the FSPGR MR sequences as the point of insertion of the infundibulum (pituitary stalk) viewed in the coronal plane (Fig. 4a). Thereafter, using the sagittal plane (so that the midline position could not be altered), the center of the gland was located (Fig. 4b).



A rectangular volume of interest was centered at this point and was used to bisect the gland (Fig. 4c). The maximum value in each side of the gland was found, and the contrast between these maximum values was taken as a measure of lateralization. This contrast was then divided by the noise (standard deviation in the normalization ROI) to give a contrast-to-noise ratio (CNR) (see Eq. 1).

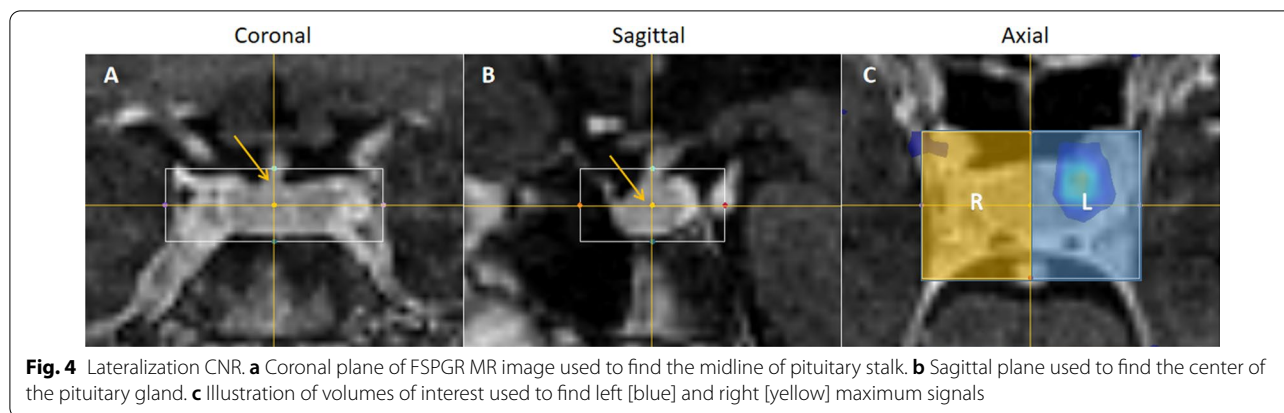


Fig. 4 Lateralization CNR. **a** Coronal plane of FSPGR MR image used to find the midline of pituitary stalk. **b** Sagittal plane used to find the center of the pituitary gland. **c** Illustration of volumes of interest used to find left [blue] and right [yellow] maximum signals

$$CNR = (Max\ Signal - Max\ Contralateral\ Signal) / Standard\ Deviation\ in\ reference\ ROI \quad (1)$$

where Max Signal can be either in the left or the right side of the pituitary gland (relative to the pituitary stalk) and the Max Contralateral Signal is from the opposite side of the gland to the Max Signal.

The mean CNR for both techniques was found, and the technique with the highest value was considered the most appropriate for highlighting the differences.

Results

Normalization

To determine the reference region to use for normalization, the mean absolute percentage difference between the maximum signal in the pituitary gland at both time points was found using three reference regions (cerebellum, gray matter and pons) and using SUVbw without normalization. The mean absolute percentage differences were found to be 2.4% for SUVr [cerebellum], 8.8% for SUVr [pons], 5.2% for SUVr [gray matter] and 23.1% for the SUVbw [no region]. The percentage differences are shown as a box plot in Fig. 5. Based on these results, the cerebellum was chosen as the reference region for normalization in the comparison of the subtraction imaging and will be known as SUVrSub [cerebellum].

Both subtraction imaging techniques and the standard clinical Met-PET scans were compared using CNR (see Eq. 1 and Fig. 5) for ten patients with a pituitary tumor that had confirmed lateralization. All three image types for all ten patients correctly lateralized to the known location of the tumor with mean CNR of 6.2, 8.1 and 11.1 for SUVbw, SUVbwSub and SUVrSub [cerebellum], respectively. Therefore on average, the SUVrSub [cerebellum] had the highest CNR with the SUVbwSub also improving detectability over SUVbw. However, although SUVrSub [cerebellum] improved detectability in all ten

patients, SUVbwSub only improved this in six subjects. Therefore in four patients, the detectability was higher for SUVbw than SUVbwSub. Figure 6 shows paired CNR measurements for both subtraction techniques compared with the original SUVbw image.

The images for a representative subject are shown in Fig. 7. This example is one of the subjects where the CNR was highest for the SUVrSub [cerebellum] and lowest for the SUVbwSub. The images highlight that the subtraction image generated from the SUVbw images is less pronounced than the normalized PET images because the SUVbw values seen in the suppressed scan are globally higher than those of the baseline scan. The inconsistency in uptake between the scans is improved by normalization, which is why the SUVrSub [cerebellum] image is much more pronounced.

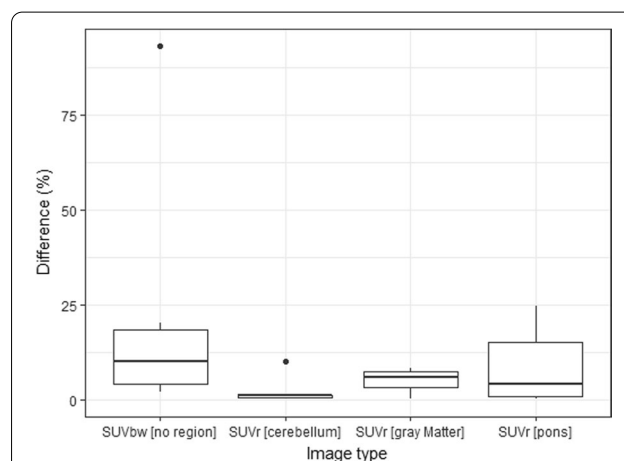
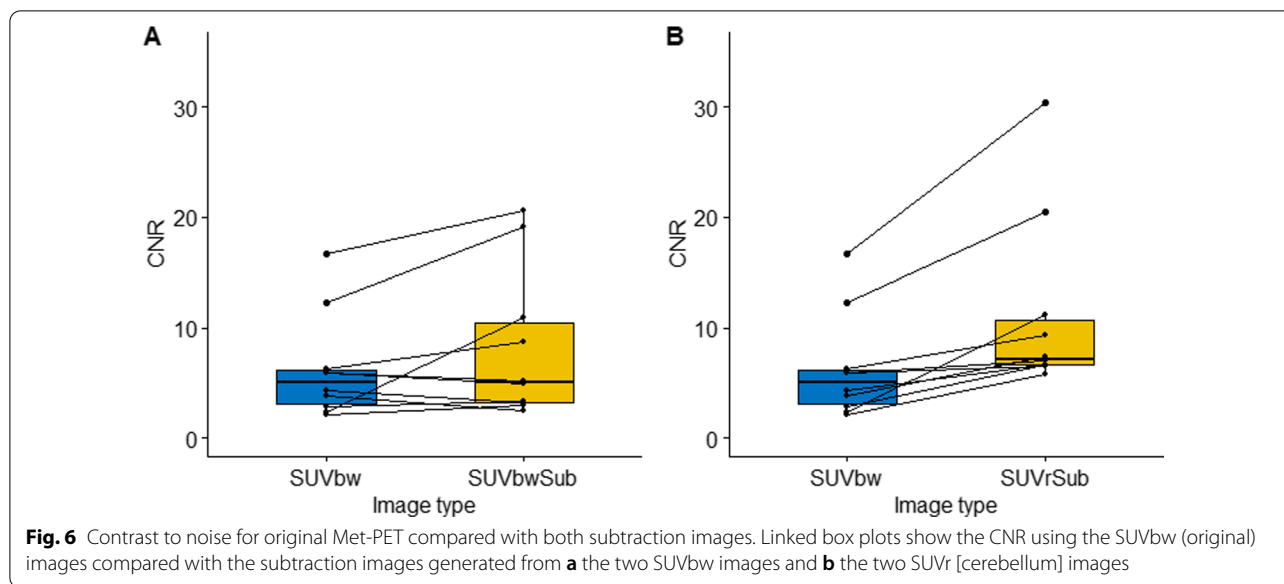


Fig. 5 Box plots of maximum signal differences. Absolute percentage differences of the maximum signal in the pituitary gland, comparing pairs of images from healthy volunteers normalized to different regions



Discussion

We have shown that subtraction imaging, generated from normalized Met-PET scans performed before and after medical suppression of tumor function, permits accurate lateralization of pituitary tumors, with an improved CNR when compared with standard clinical imaging.

The registration process was optimized for direct registration between the PET and MRI images (Fig. 1), without the need for a hybrid CT. This reduced the computational time required for the process and, more importantly, negates the need for additional registrations when there are small misalignments between the PET and the hybrid CT. These misregistrations happen infrequently and are easily seen by expert reviewers in standard clinical practice due to physiological uptake in surrounding structures (e.g., gray matter, bone marrow). However, these misalignments would not be as easily seen in the subtraction image, because much of the surrounding uptake is suppressed and therefore direct registration between PET and MRI is considered an important part of the overall process.

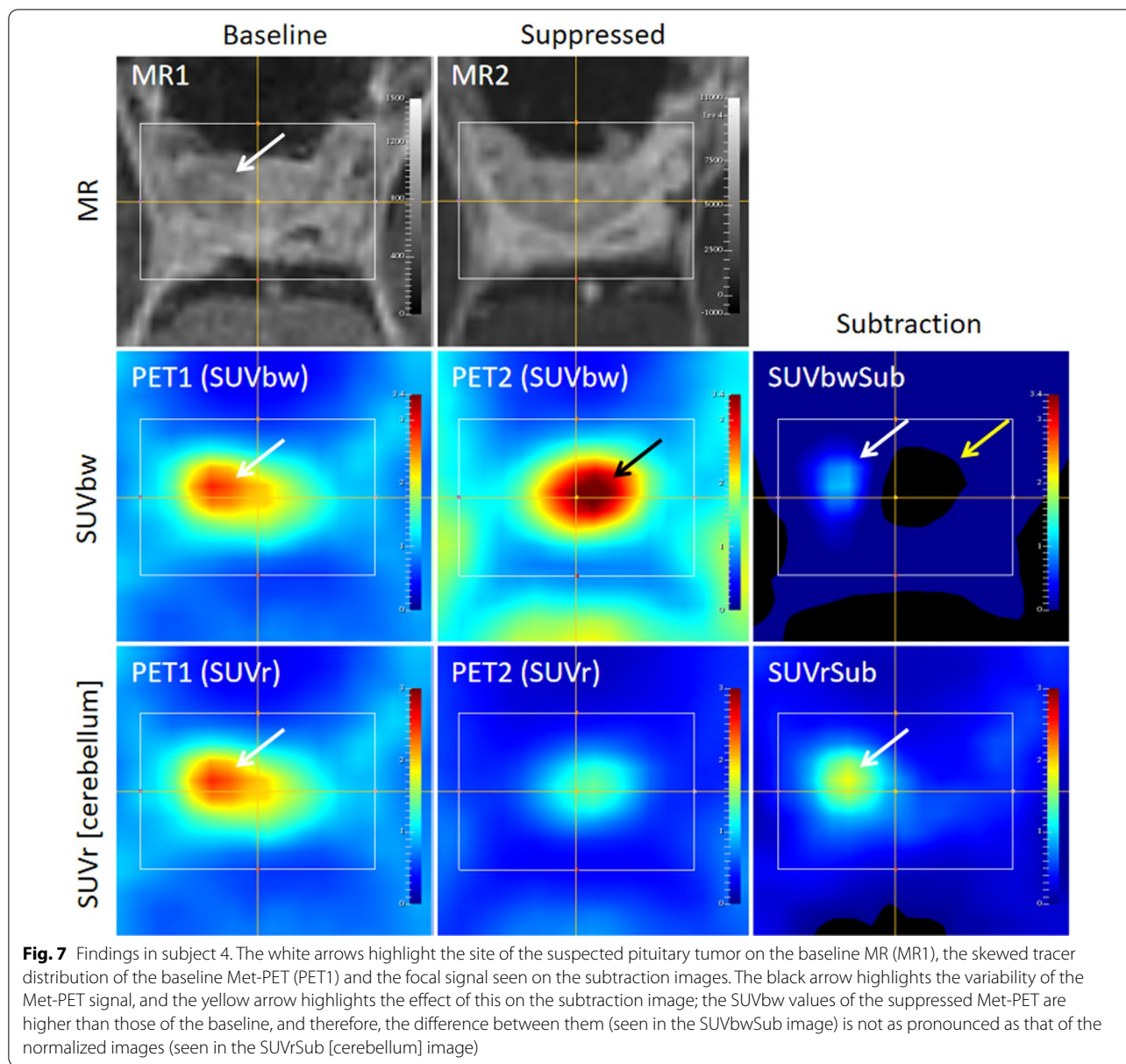
The process of creating subtraction images (Fig. 1, step 4) required additional registration between PET2 and PET1 because although the steps of the initial registration (Fig. 1, steps 1–3) result in the four images being aligned, the subtraction process will highlight any small differences caused by minor misalignments. This additional registration typically took less time (<10 s) than the other registration steps (1–3) because both images are smaller than the MRI images.

The PET2 to PET1 registration was also used to resample the PET2 image into an identical matrix as PET1 (Fig. 1). These identical matrices are crucial to be able to

perform voxel-wise calculations. Attempts to create the subtraction images by using the world coordinate system were not as successful because the same interpolation of the voxel values was still required but had to be performed as part of the subtraction process and added unnecessary computational complexity.

The process of normalization involved outlining the reference region using a semi-automated (using a thresholding tool) method. Therefore, outlining these regions could be improved by automating the process using artificial intelligence (AI). There is a growing body of work that shows that AI and in particular deep-learning techniques (DL) have potential in automatically segmenting various areas of the body including the cerebellum [26].

To assess which reference region would be used for normalization, we compared the maximum signal in the pituitary gland using two images from each of the healthy volunteers acquired at different time points. As well as the regions we also compared the differences seen in the original SUVbw images in case no reference region was needed. We found that the maximum signal from the SUVbw images could vary on average by more than 20% (see Fig. 5). Differences of this magnitude are critical when creating images to highlight differences between pairs of datasets, but are arguably even more important in clinical practice when a patient is returning for surveillance imaging. Therefore, it could be recommended that all Met-PET images are normalized using a reference ROI before reading, although more data would be needed to confirm our findings. Using the six healthy volunteers, our results indicate that all three reference regions (cerebellum, gray matter and pons) reduce the variation in maximum pituitary gland signal when compared to



non-normalized SUVbw images (Fig. 6). Using the cerebellum led to the lowest variations and consequently was selected when creating the subtraction images from normalized datasets. These normalized datasets were compared with the original (non-normalized) datasets to find the technique that resulted in the highest detectability of the tumor (as defined by Eq. 1).

Quantifying the CNR between the left and right side of the pituitary gland (Fig. 4) acted as a good surrogate for lateralization, correctly locating the tumor side in all cases for all three image types (SUVbw, SUVbwSub and SUVrSub [cerebellum]). Although it performed well, it was still limited because it only considered the pixel with

maximum intensity from each side. Other metrics, such as the mean signal and absolute signal on each side, were ineffective in comparing the subtraction imaging techniques because they did not account for the noise in the image. Since the noise in the images varied and was not comparable between techniques, taking into account this noise was especially important when comparing those techniques that had very high or very low signal. Only by comparing the contrast between the PET signal and noise, we were able to analyze the techniques in a meaningful way.

The CNR results indicate that normalized subtraction imaging (SUVrSub [cerebellum]) improved detectability

of pituitary adenomas when directly compared to the original (SUVbw) images and non-normalized (SUVbwSub) images. In every case, the SUVrSub [cerebellum] image had the highest CNR out of the three image sets, but importantly the SUVbwSub images did not always generate a higher CNR over SUVbw images. In four out of the ten patients, the CNR was lower after subtraction which highlights the importance of normalization.

This technique could also find application with other pituitary tumor subtypes where there is the possibility to suppress tumor function using medical therapy (for example, prolactinoma scanned pre- and post-dopamine agonist therapy; acromegaly scanned pre- and post-somatostatin receptor ligand). Similarly, the basic principles underpinning our methodology are potentially applicable to other PET ligands and other tumors. In particular, PET ligands that target tumoral SSTR receptor expression in TSH-secreting pituitary adenomas may be considered [27] although the use of SRL therapy to suppress PET uptake may not yield the same results seen in this study with Met-PET because the 'cold' ligand will directly compete with the PET ligand for somatostatin receptor binding sites.

Conclusion

In conclusion, this study demonstrates that pituitary adenoma localization can be aided by normalized subtraction imaging. By highlighting areas of change between a baseline Met-PET image and registered suppressed Met-PET, this novel technique can allow improved localization of an adenoma when compared with conventional imaging modalities, especially when the cerebellum is used as a reference region. Implementation of this technique in clinical practice may be of particular added value when definitive intervention (e.g., transsphenoidal pituitary surgery or stereotactic radiosurgery) is being considered, to guide targeted intervention and mitigate the risk of disrupting normal pituitary gland function.

Abbreviations

AC: Attenuation correction; AI: Artificial intelligence; CoV: Coefficient of variation; CNR: Contrast-to-noise ratio; Co-Reg: Co-registration of two or more images; CT: X-ray computed tomography; FSPGR: Type of MRI imaging—fast spoiled gradient (recalled) echo; Met-PET: ¹¹C-methionine PET; MRI: Magnetic resonance imaging; OSEM: Ordered subset expectation maximization; PA: Pituitary adenoma; PET: Positron emission tomography; SRL: Somatostatin receptor ligand; SUV: Standardized uptake value; SUVbw: Standardized uptake value image using body weight; SUVr: Standardized uptake value ratio; SUVbwSub: Subtraction image generated from SUVbw images; SUVrSub: Subtraction image generated from SUVr images; TE: Echo time used in MRI; TOF: Time of flight; TR: Repetition time used in MRI; TSS: Transsphenoidal pituitary surgery; VOI: Volume of interest.

Acknowledgements

The authors would like to acknowledge Professor Franklin Aigbirhio, Dr Istvan Boros, Dr Stefan Hader and Dr Lei Li from the radiochemistry group at the

Wolfson Brain Imaging Centre for their help in producing the radiopharmaceuticals used in this work.

Author contributions

DG, RS, JM, OK, AK, RM, WB and MG developed the initial project design. DG, RS, JM, RC, BG, NB, SH, LA, IM, HC, WB and MG contributed to the data processing. DG, RS, JM, RC, BG, MvdM, AP, NB, SH, IM, LA, RM, HC, WB and MG contributed to the data presentation and writing of the manuscript. DG, RS, JM, MvdM, RC, BG, WB and MG contributed to the figures. All authors read and approved the final manuscript.

Funding

This research was supported by the NIHR Cambridge Biomedical Research Centre (BRC-1215-20014). The views expressed are those of the author(s) and not necessarily those of the NIHR or the Department of Health and Social Care.

Availability of data and materials

The datasets used and/or analyzed during the current study are available from the corresponding author on reasonable request.

Declarations

Ethics approval and consent to participate

Informed consent was obtained from all individual participants included in the study. This study was performed in line with the principles of the Declaration of Helsinki. Approval was granted by the National Research Ethics Service (NRES) London Fulham Committee (28/9/14—Reference: 14/LO/1642).

Consent for publication

Not applicable.

Competing interests

The authors declare that they have no competing interests.

Author details

¹Department of Nuclear Medicine, Cambridge University Hospitals NHS Foundation Trust, Cambridge Biomedical Campus, Hills Road, Cambridge CB2 0QQ, UK. ²Cambridge Endocrine Molecular Imaging Group, University of Cambridge, Addenbrooke's Hospital, Cambridge Biomedical Campus, Hills Road, Cambridge CB2 0QQ, UK. ³East Anglian Regional Radiation Protection Service, Cambridge University Hospitals NHS Foundation Trust, Cambridge Biomedical Campus, Hills Road, Cambridge CB2 0QQ, UK. ⁴Division of Neurosurgery, Department of Clinical Neurosciences, University of Cambridge & Addenbrooke's Hospital, Cambridge CB2 0QQ, UK. ⁵Department of Radiology, University of Cambridge, Cambridge Biomedical Campus, Hills Road, Cambridge CB2 0QQ, UK. ⁶Metabolic Research Laboratories, Wellcome-MRC Institute of Metabolic Science University of Cambridge, National Institute for Health Research Cambridge Biomedical Research Centre, Addenbrooke's Hospital, Hills Road, Cambridge CB2 0QQ, UK.

Received: 7 January 2022 Accepted: 25 April 2022

Published online: 07 May 2022

References

- Kopczak A, Renner U, Karl SG. Advances in understanding pituitary tumors. *F1000Prime Rep.* 2014;6:5.
- Bashari WA, Senanayake R, Fernández-Pombo A, Gillett D, Koulouri O, Powlson AS, et al. Modern imaging of pituitary adenomas. *Best Pract Res Clin Endocrinol Metab.* 2019;33(2): 101278.
- Johnson MD, Woodburn CJ, Vance ML. Quality of life in patients with a pituitary adenoma. *Pituitary.* 2003;6(2):81–7.
- Andela CD, Scharloo M, Pereira AM, Kaptein AA, Biermasz NR. Quality of life (QoL) impairments in patients with a pituitary adenoma: a systematic review of QoL studies. *Pituitary.* 2015;18(5):752–76.
- Freda PU, Beckers AM, Katznelson L, Molitch ME, Montori VM, Post KD, et al. Pituitary incidentaloma: an endocrine society clinical practice guideline. *J Clin Endocrinol Metab.* 2011;96(4):894–904.

6. Nieman LK. Cushing's syndrome: update on signs, symptoms and biochemical screening. *Eur J Endocrinol.* 2015;173(4):M33–8.
7. Katznelson L, Laws ER Jr, Melmed S, Molitch ME, Murad MH, Utz A, et al. Acromegaly: an endocrine society clinical practice guideline. *J Clin Endocrinol Metab.* 2014;99(11):3933–51.
8. Koulouri O, Steuwe A, Gillett D, Hoole AC, Powlson AS, Donnelly NA, et al. A role for 11C-methionine PET imaging in ACTH-dependent Cushing's syndrome. *Eur J Endocrinol.* 2015;173(4).
9. Koulouri O, Hoole AC, English P, Allinson K, Antoun N, Cheow H, et al. Localisation of an occult thyrotropinoma with 11 C-methionine PET-CT before and after somatostatin analogue therapy. *Lancet Diabetes Endocrinol.* 2016;4(12):1050.
10. Bashari WA, Senanayake R, Fernandez-Pombo A, Gillett D, Koulouri O, Powlson A, et al. Extended TSS (guided by 11C-methionine PET + MRI (Met-PET/MRCR)) can be an effective treatment option for patients with persistent acromegaly due to previously deemed unresectable lateral disease. In *BioScientifica*; 2019 [cited 2020 May 15]
11. Bonert V, Mirocha J, Carmichael J, Yuen KCJ, Araki T, Melmed S. Cost-effectiveness and efficacy of a novel combination regimen in acromegaly: a prospective. *Randomized Trial J Clin Endocrinol Metab.* 2020;105(9):e3236–45.
12. Gatto F, Barbieri F, Gatti M, Wurth R, Schulz S, Ravetti J-L, et al. Balance between somatostatin and D2 receptor expression drives TSH-secreting adenoma response to somatostatin analogues and dopastatins. *Clin Endocrinol (Oxf).* 2012;76(3):407–14.
13. Hassler S, Ben-Sellem D, Hubele F, Constantinesco A, Goetz C. Dual-isotope 99mTc-MIBI/123I parathyroid scintigraphy in primary hyperparathyroidism: comparison of subtraction SPECT/CT and pinhole planar scan. *Clin Nucl Med.* 2014;39(1):32–6.
14. Desai A, Bekelis K, Thadani VM, Roberts DW, Jobst BC, Duhaime A-C, et al. Intercital PET and ictal subtraction SPECT: Sensitivity in the detection of seizure foci in patients with medically intractable epilepsy. *Epilepsia.* 2013;54(2):341–50.
15. Haginoya K, Uematsu M, Munakata M, Kakisaka Y, Kikuchi A, Nakayama T, et al. The usefulness of subtraction ictal SPECT and ictal near-infrared spectroscopic topography in patients with West syndrome. *Brain Dev.* 2013;35(10):887–93.
16. Koo CW, Devinsky O, Hari K, Balasny J, Noz ME, Kramer EL. Stratifying differences on ictal/interictal subtraction SPECT images. *Epilepsia.* 2003;44(3):379–86.
17. Tan KM, Britton JW, Buchhalter JR, Worrell GA, Lagerlund TD, Shin C, et al. Influence of subtraction ictal SPECT on surgical management in focal epilepsy of indeterminate localization: a prospective study. *Epilepsy Res.* 2008;82(2):190–3.
18. Marcoux A, Burgos N, Bertrand A, Teichmann M, Routier A, Wen J, et al. An automated pipeline for the analysis of PET data on the cortical surface. *Front Neuroinform.* 2018;12:2. <https://doi.org/10.3389/fninf.2018.00094/full>.
19. Perissinotti A, Setoain X, Aparicio J, Rubí S, Fuster BM, Donaire A, et al. Clinical role of subtraction ictal SPECT coregistered to MR imaging and 18F-FDG PET in pediatric epilepsy. *J Nucl Med.* 2014;55(7):1099–105.
20. López-González FJ, Silva-Rodríguez J, Paredes-Pacheco J, Niñerola-Baizán A, Efthimiou N, Martín-Martín C, et al. Intensity normalization methods in brain FDG-PET quantification. *Neuroimage.* 2020;15(222): 117229.
21. Garali I, Adel M, Bourennane S, Guedj E. Region-based brain selection and classification on pet images for Alzheimer's disease computer aided diagnosis. In: 2015 IEEE international conference on image processing (ICIP). 2015. p. 1473–7.
22. Gurnell M, Koulouri O, Bashari W. Thyrotropinomas. In: Owen K, Turner H, Wass J, editors. *Oxford handbook of endocrinology & diabetes.* 4th ed. Oxford: Academic Press; 2022. p. 255–63.
23. Koulouri O, Gurnell M. TSH-secreting pituitary adenomas. In: Huhtaniemi I, Martini L, editors. *Encyclopedia of endocrine diseases, vol. 2.* 2nd ed. Oxford: Academic Press; 2019. p. 261–6.
24. Illouz F, Chanson P, Sonnet E, Brue T, Ferriere A, Raffin Sanson ML, Vantghem MC, Raverot G, Munier M, Rodien P, Briet C. Somatostatin receptor ligands induce TSH deficiency in thyrotropin-secreting pituitary adenoma. *Eur J Endocrinol.* 2021;184(1):1–8. <https://doi.org/10.1530/EJE-20-0484>.
25. Fedorov A, Beichel R, Kalpathy-Cramer J, Finet J, Fillion-Robin J-C, Pujol S, et al. 3D Slicer as an image computing platform for the Quantitative Imaging Network. *Magn Reson Imaging.* 2012;30(9):1323–41.
26. Xiong X, Linhardt TJ, Liu W, Smith BJ, Sun W, Bauer C, et al. A 3D deep convolutional neural network approach for the automated measurement of cerebellum tracer uptake in FDG PET-CT scans. *Med Phys.* 2020;47(3):1058–66.
27. Tjörnstrand A, Casar-Borota O, Heurling K, et al. Pre- and postoperative 68Ga-DOTATOC positron emission tomography for hormone-secreting pituitary neuroendocrine tumours. *Clin Endocrinol (Oxf).* 2021;00:1–12. <https://doi.org/10.1111/cen.14425>.

Publisher's Note

Springer Nature remains neutral with regard to jurisdictional claims in published maps and institutional affiliations.

Submit your manuscript to a SpringerOpen[®] journal and benefit from:

- Convenient online submission
- Rigorous peer review
- Open access: articles freely available online
- High visibility within the field
- Retaining the copyright to your article

Submit your next manuscript at ► [springeropen.com](https://www.springeropen.com)